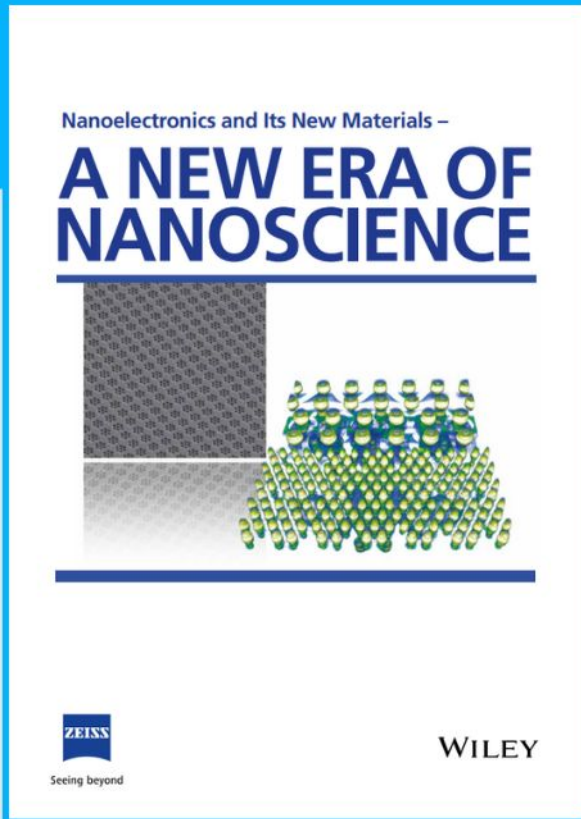




Nanoelectronics and Its New Materials – A NEW ERA OF NANOSCIENCE



Discover the recent advances in electronics research and fundamental nanoscience.

Nanotechnology has become the driving force behind breakthroughs in engineering, materials science, physics, chemistry, and biological sciences. In this compendium, we delve into a wide range of novel applications that highlight recent advances in electronics research and fundamental nanoscience. From surface analysis and defect detection to tailored optical functionality and transparent nanowire electrodes, this eBook covers key topics that will revolutionize the future of electronics.

To get your hands on this valuable resource and unleash the power of nanotechnology, simply download the eBook now. Stay ahead of the curve and embrace the future of electronics with nanoscience as your guide.



Seeing beyond

WILEY

Dilation-Responsive Microshape Programing Prevents Vascular Graft Stenosis

Se Won Yi, Young Min Shin, Jung Bok Lee, Ju Young Park, Dae-Hyun Kim, Wooyeol Baek, Jeong-Kee Yoon, Deok Gie Kim, In Sik Shin, Chang-Soo Kim, Mi-Lan Kang, Jae Won Yang,* and Hak-Joon Sung*

Shape memory materials have been successfully applied to minimally invasive implantation of medical devices. However, organ-movement-specific shape programing at a microscale level has never been demonstrated despite significant unmet needs. As vein-to-artery grafting induces vein dilation and stenosis, a polymeric self-enclosable external support (SES) is designed to wrap the vascular out-wall. Its micropores are programmed to increase sizes and interconnections upon dilation. Vessel dilation promotes venous maturation, but overdilation induces stenosis by disturbed blood flow. Therefore, the unique elastic shape-fixity of SES provides a foundation to enable a stable microscale shape transition by maintaining the vein dilation. The shape transition of micropore architecture upon dilation induces beneficial inflammation, thereby regenerating vasa vasorum and directing smooth muscle cell migration toward adventitia with the consequent muscle reinforcement of veins. This game-changer approach prevents the stenosis of vein-to-artery grafting by rescuing ischemic disorders and promoting arterial properties of veins.

macroscale level. Indeed, further progress is required so that elastic reversible material properties can be produced to handle the continuous movement of organs or tissues in the body, and the microscale resolution of design parameters can be achieved to regulate cellular-level events. Hence, we have made a significant progress in applying an advanced shape memory polymer (SMP) to develop an out-wall wrapping device (i.e., self-enclosable external support: SES) rather than popular endovascular stents aiming to address the following issues.

First, grafting two different types of vessels (e.g., vein-to-artery and synthetic-tube-to-artery) has inherent issues pertaining to the mismatch of mechanical properties and inner diameters. Consequently, hemodynamic changes are


induced with cellular dysfunctions,^[2] which serve as a major foundation for stenosis. As one of the most popular cases, when a vein is grafted to an artery (e.g., arteriovenous fistula (AVF)), venous dilation is required for contractile wall maturation, but excess circumferential dilation (>3 times) produces disturbed flow formation, leading to lumen occlusion.^[3] The unique elastic shape fixity function of SMP based on SES controls the

1. Introduction

Shape memory materials enable minimally invasive implantation of vascular devices.^[1] However, such current devices mainly use a simple shape transition from pre- to postdeployment (e.g., circumferential expansion, bending, widening, and tilting), and this one-way shape transition is irreversible and occurs at a

Dr. S. W. Yi, J. Y. Park, Dr. M.-L. Kang
TMD LAB Co., Ltd.
6th floor, 31, Gwangnaru-ro 8-gil, Seongdong-gu, Seoul 04799,
Republic of Korea

Dr. Y. M. Shin, Dr. D.-H. Kim, Dr. J.-K. Yoon, Prof. H.-J. Sung
Department of Medical Engineering
Yonsei University College of Medicine
50-1 Yonsei-ro, Seodaemun-gu, Seoul 03722, Republic of Korea
E-mail: hj72sung@yuhs.ac

 The ORCID identification number(s) for the author(s) of this article can be found under <https://doi.org/10.1002/smll.202007297>.

© 2021 The Authors. Small published by Wiley-VCH GmbH. This is an open access article under the terms of the Creative Commons Attribution-NonCommercial-NoDerivs License, which permits use and distribution in any medium, provided the original work is properly cited, the use is non-commercial and no modifications or adaptations are made.

DOI: 10.1002/smll.202007297

Prof. J. B. Lee
Department of Biological Science
Sookmyung Women's University
Cheongpa-ro 47-gil 100, Yongsan-gu, Seoul 04310, Republic of Korea

W. Baek
Department of Plastic and Reconstructive Surgery
Yonsei University College of Medicine
50-1 Yonsei-ro, Seodaemun-gu, Seoul 03722, Republic of Korea

D. G. Kim, I. S. Shin
Department of Surgery
Yonsei University Wonju College of Medicine
Wonju 220-701, Republic of Korea

Dr. C.-S. Kim
Numais Co., Ltd.
5th floor, 31, Gwangnaru-ro 8-gil, Seongdong-gu, Seoul 04799,
Republic of Korea

Prof. J. W. Yang
Division of Nephrology, Department of Nephrology
Yonsei University Wonju College of Medicine
Wonju 220-701, Republic of Korea
E-mail: kidney74@yonsei.ac.kr

vessel-dilation-mediated hemodynamic change in vein-to-artery grafting.

Second, the efficient cooperation of micropores (150–500 μm) and their interconnectivity induces beneficial inflammatory response and consequent microvessel growth (angiogenesis).^[4] Therefore, the shape programming of micropores generates beneficial inflammatory signals from the out-wall of the vessel, thereby guiding the migration of smooth muscle cells (SMCs) toward adventitia rather than inducing an intimal hyperplasia like a mitogen.^[5] Meanwhile, for grafting, washing the vein damages vasa vasorum and, thus, induces ischemic disorders^[6] with pathological SMC actions,^[7] which was also rescued by the angiogenesis-inducible beneficial inflammation. These rationales justify the SES approach with the vein-dilation-responsive shape programming of micropore architecture to prevent vascular occlusion.

2. Results

2.1. Dilation-Responsive Microscale Shape Programming of the External Wrapping Device (SES)

SMP and gelatin porogen were used to produce the porous SES through a series of tuning steps, including crosslinking, porogen leaching with punching, and shape programming processes (Figure 1a, top). A self-enclosable property promotes a precision level of shape fixity as changes in the size and geometry of a target vessel before and after vessel dilation can be precalculated (Figure 1a, bottom). This advantage enables the user-specified control of vein dilation and subsequent transition of a micropore-shaping program to promote the regeneration of vasa vasorum by facilitating the in-and-out transport of nutrients and oxygen around the vascular out-wall. Thus, these functions can be enhanced because the dilation-responsive increase in pore sizes with thickness compression (Poisson's ratio) and inner pore-wall crushing promotes the pore interconnectivity.

As wrapping should be performed immediately after the SES placement to minimize operation time and consequent infection possibility, the shape recovery temperature ($=T_m$) was set to slightly below 37 $^{\circ}\text{C}$ by controlling the crosslinking time (Figure 1b). An increase in the degree of crosslinking reduces the crystallinity of SMPs, thereby decreasing T_m .^[8] Moreover, SES can manage consistent stress to the poly(dimethylsiloxane) (PDMS)-compatible level when exposed to 10% cyclic strain after several cycles of stabilization step and then up to 20 000 times (Figure 1c). Since PDMS is one of the most well-known elastic materials and its mechanical properties have been characterized extensively,^[9] it was used as a control to compare the ability to manage repeated stress with that of SES. In addition, 10% strain was applied following the dilation ratio of rabbit carotid artery as determined through filming, image capture, and image analysis (Figure 1c, top). The result proves the excellent fatigue resistance of SES to synchronize with continuous arterial contractions upon wrapping. Moreover, the porosity was maximized up to an average of 60% by varying the amount of gelatin porogen and punching (P : 400 μm) as small and large microporogens, respectively (Figure 1d). Parameters pertaining to micropores were set to maintain the stress at 0.2–0.25 MPa and \approx 99% of shape recovery, without losing the trend of incremental strain at break (Table S1, Supporting Information).

When the model was dilated (Dil) by 2.5 times from the temporary shape (Tem), the optical confocal images exhibited merging between the two neighboring pores as an indication of increasing the pore interconnectivity (Figure 1e -i). This result was supported by \approx 25% decrease in the SES thickness in alignment with Poisson's ratio rule as well as \approx 50% increase in the areas of small and large micropores (Figure 1e -ii). Moreover, the major and minor axes of large micropores increased by \approx 20% while the axes of small micropores increased by \approx 50% (Figure S1, Supporting Information). These results indicate cooperative functions of large and small micropores because the ellipsoidal expansion of large micropores significantly improved the pore interconnectivity while the dilation-mediated crushing of small micropores served as void bridges to facilitate the merging process between neighboring large pores (Figure 1f). The size range of small micropores has been reported to induce beneficial inflammation by which angiogenesis can be promoted,^[10,11] and the large micropores are expected to provide rooms for volumetric expansion of SES as well as growth of microvessels. These unique functions of large and small micropores validate the unprecedented design concept of dilation-responsive microscale shape programming.

2.2. Regenerative Inflammation as a Causative Mechanistic Factor and Reinforcement of SMC Layer and Vasa Vasorum in Vein Graft (VG)

The acute phase inflammation arises inevitably upon the implantation of medical devices owing to tissue incision and foreign materials introduction. If regenerative inflammation is activated progressively, vessel growth is induced with guiding cell migration.^[12,13] As SES was designed to activate regenerative inflammation by the micropore architecture, the *in vitro* model of RAW 264.7 macrophage activation under the lipopolysaccharide (LPS) treatment was first used to determine the micropore effects (Figure 2a). Compared with the other test substrates, the SMP pore-mediated generation of noneven narrow surfaces appeared to limit macrophage spreading and subsequent activation (Figure 2a) as supported by the least cell aspect ratio (spreading) (Figure S2, Supporting Information). Moreover, the matrix stiffness decreased drastically from coverslip to flat SMP and significantly further to porous SMP (Figure 2b), leading to the highest expression levels of regenerative inflammation genes (Figure 2c) in agreement to previous studies.^[14–16] Along the same line, the porous SMP group exhibited i) the highest levels of gene expression in the proangiogenesis (Figure 2d) and vascular SMC mitogen markers (Figure 2e), ii) the highest secretion level of combined marker proteins in each category of regenerative M2 activation, proangiogenesis, and vascular SMC mitogen (Figure S3, Supporting Information), and iii) the increased protein expression of CD206 (M2 marker), as opposed to that of inducible nitric oxide synthase (iNOS, M1 marker) (Figure S4, Supporting Information) among the test groups.

The SMP substrate managed cell viability, proliferation, and circularity to the levels of the tissue culture polystyrene (TCPS) upon the culture of human aortic SMCs despite significantly less adhesion (Figures S5 and S6, Supporting Information), indicating no abnormal change of SMC phenotype. In order to further examine the beneficial inflammatory effect of porous SMP, conditioned

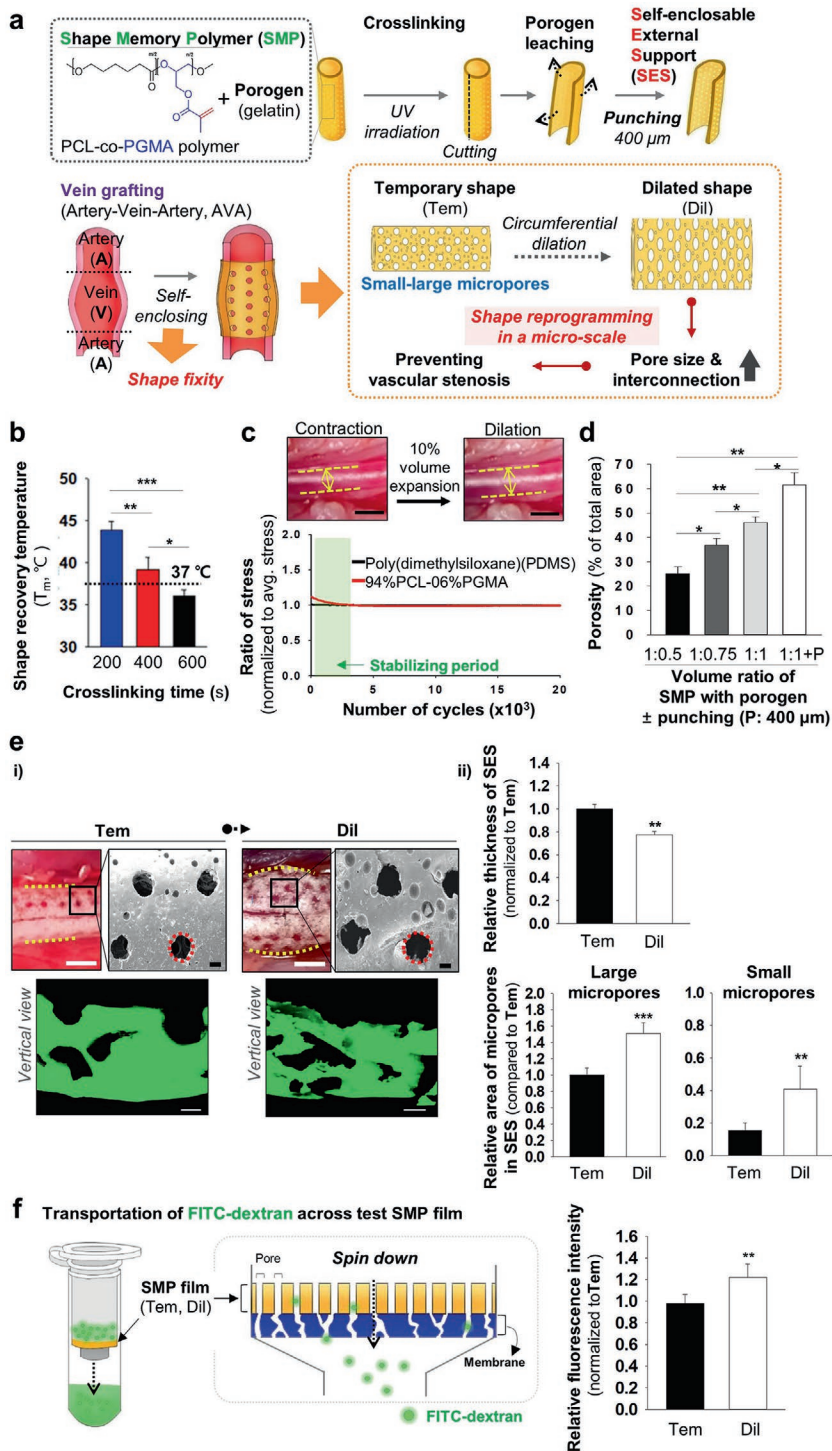


Figure 1. Concept and characterization of self-enclosable external support (SES). a) Illustration of SES fabrication (top) with a shape memory polymer (SMP) and its deployment (bottom) by self-enclosing (wrapping) AVA graft in end-to-end anastomosis at near body temperature. Upon wrapping the AVA graft, the SES dilates along the circumferential direction by vessel dilation. Consequently, the size and area of small and large micropores increase, thereby improving the pore interconnectivity. We hypothesize that this microscale control prevents vascular stenosis by rescuing ischemic disorders and promoting arterial properties of vein. b) A controllable spectrum of T_m for shape recovery as a function of UV exposure-mediated crosslinking time (200, 400, and 600 s) ($N = 3$). c) The 10% dilation ratio of rabbit carotid artery was determined through filming, image capture, and image analysis. Poly(dimethylsiloxane)

media (CM) were collected from monocyte (RAW 264.7) culture on the three test groups and then treated to ECs and vascular SMCs (Figure 2f). Consequently, the CM of porous SMP promoted in vitro tubulogenesis of ECs most among the test groups as presented by the quantitative parameters (Figure 2g). These results were also supported by the ex vivo aortic ring assay (Figure S7, Supporting Information) as vasa vasorum growth was merely triggered by LPS treatment but significantly promoted by SES. Moreover, SMC migration was promoted along the same line when the cell number in the migration area was tracked for 24 h after moving to the designated area (Figure 2h). The CM of porous SMP guided the direction of SMC migration similar to a chemoattractant, as demonstrated by Boyden chamber assay (Figure 2i). These results indicate a promising potential for SES in guiding the SMC migration to reinforce out-wall muscle instead of triggering intimal hyperplasia as well as in effectively regenerating vasa vasorum to rescue ischemic disorders.

2.3. Attenuating Vein Dilation as a Promoter of Antistenotic Effect

The regulatory effect of SES on the ex vivo dilation of the rabbit jugular vein (Figure 3a) was clearly evidenced by the higher dilation ratio (≈ 3 times) and compliance (≈ 7 -6) without (w/o) SES compared with those (≈ 2 times and 4.2×10^{-6}) with (w/) SES when the input flow pressure was increased gradually (0–160 mmHg) (Figure 3b). The computational fluid dynamic (CFD) analysis supported these experimental results by confirming the maximum ratio of vein dilation to minimize the stenotic flow disturbance^[17–19] when the dilation degree varied (Figure 3c) and the hexahedron CFD mesh

(PDMS)-compatible fatigue property of SMP film under consecutive cyclic strain up to 20 000 times in dynamic mechanical analyzer (DMA). d) Controlling the porosity of SES by altering the volume ratio between porogen (gelatin) and SMP solutions ± punching (P: 400 μm) ($N = 4$). e-i) The confocal images show the dilation-mediated changes of micropores with analyses of e-ii) the relative support thickness and large–small micropore areas before wrapping (temporary: Tem) and after dilation (Dil). Scale bar = 2 mm (optical images) and 200 μm (confocal images). f) A consequent dilation-mediated increase in pore interconnectivity from Tem to Dil by spinning down fluorescein isothiocyanate-conjugated dextran (FITC–dextran) across test films (transportation test, $N = 6$). * $p < 0.05$, ** $p < 0.01$, and *** $p < 0.001$ between comparison groups.

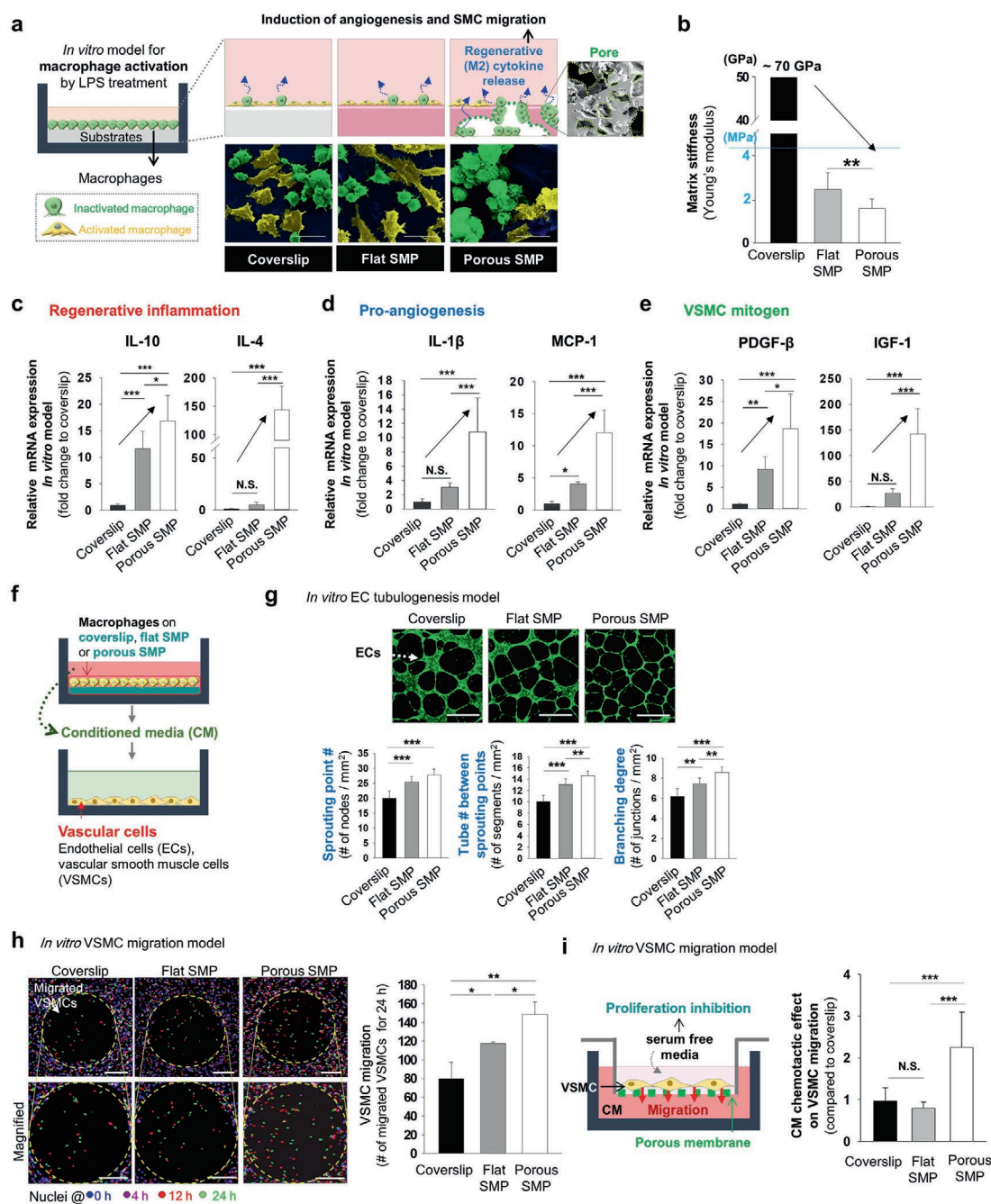


Figure 2. Causative effects of the SES pore structure on regenerative inflammation, vasa vasorum regeneration, and muscle reinforcement (arterialization) of vein graft. a) Illustration of in vitro model with mechanistic insight into the inhibitory effect of pore structure on macrophage spreading and consequent destructive activation. Mouse macrophages (RAW 264.7) were cultured on the test substrates (coverslip glass, flat SMP, and porous SMP) and activated by the treatment of lipopolysaccharide (LPS) for 3 days. The SEM images show spreading (activated, yellow) and nonspreading (inactivated, green) morphologies of macrophages on the test substrates. Scale bar = 20 μ m. b) Matrix modulus of test matrix types. c–e) (In vitro model in (a)) Marker gene expression in macrophages for c) regenerative inflammatory activation (IL-10 and IL-4), d) proangiogenesis (IL-1 β and MCP-1), and e) VSMCs mitogen (PDGF- β and IGF-1) ($N = 3$). f) Schema of in vitro model to investigate the beneficial inflammatory (M2) effect of pore structure on vascular cell responses. Macrophages (RAW 264.7) were cultured on the test substrates (coverslip, flat SMP, and porous SMP) under activation by the LPS treatment for 48 h. Then, the conditioned media (CM) were treated to endothelial cells (ECs) and vascular smooth muscle cells (VSMCs). g–i) (In vitro model in (f)) g) Tubulogenesis of human umbilical vein ECs (HUVECs; phalloidin 488 green) at 8 h postculture on Matrigel under the test CM treatment. Then, sprouting point, tube number, and branching degree (number of nodes, segments, and junctions per mm², respectively, $N = 3$) were quantitatively analyzed. Scale bar = 200 μ m. h) Migration of human aortic VSMCs into the empty center region (circle in top row) at 0 h (blue), 4 h (purple), 12 h (red), and 24 h (green) postculture under the test CM treatment. The migration areas were magnified (bottom row), and the number of migrated VSMCs for 24 h was determined. i) Promotive effects of the CMs from the test material types on the migration of human aortic VSMCs were compared by Boyden chamber assay for 24 h ($N = 3$). b–i) * $p < 0.05$, ** $p < 0.01$, and *** $p < 0.001$ between comparison groups or versus w/o SES.

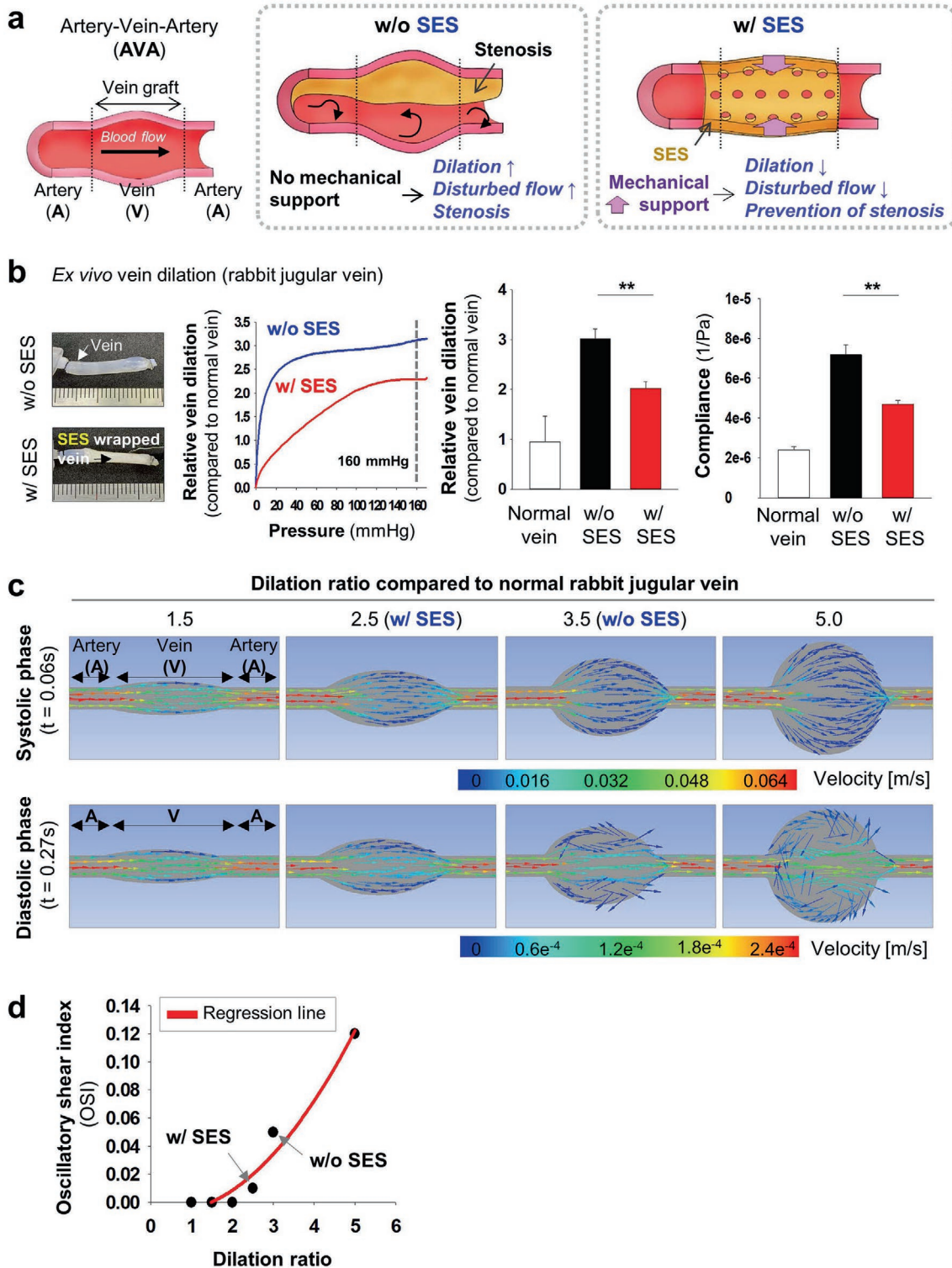


Figure 3. Reduction of vein dilation in an AVA grafting model by SES with consequent attenuation of disturbed flow formation. a) Illustration of working mechanism for SES deployment to reduce vein dilation by a mechanical support and thereby prevent stenosis. b) (Left-digital photos) Ex vivo comparison between w/ and w/o SES in the dilation of rabbit jugular veins at 160 mmHg of flow injection pressure. The dilation degrees of two test groups relative to normal were profiled when the injection pressure increased gradually from 0 to 160 mmHg. (Right graphs) Vein dilation was quantitatively analyzed regarding diameter and compliance, followed by normalization to the average values of normal vein ($=1$) ($N = 3$). $**p < 0.01$, between comparison groups. c) In accordance with variation of vein dilation ratio in AVA grafting, computational fluid dynamic (CFD) modeling of blood flow patterns and d) calculation of time-averaged oscillatory shear index (OSI), indicating a drastic increase of flow oscillation in w/o SES (dilation ratio >3) while preventing the antidilation effect of SES.

morphology was used (Figure S8, Supporting Information). The reported pulsatile waveform with a peak inflow velocity of 0.04 m s^{-1} and 3.33 Hz (Figure S9, top, Supporting Information)^[20] was used to present the systolic and diastolic flow pattern vectors at simulation times of $t = 0.06 \text{ s}$ and $t = 0.27 \text{ s}$, respectively (Figure 3c). As a result, the systolic flow patterns were laminar overall, even when the dilation ratio increased by 5.0 times. However, the diastolic increase of vessel dimension from 2.5 (w/ SES) to 3.5 times (w/o SES) resulted in a substantial oscillatory flow formation, being most disturbed at the 5.0 dilation ratio. The wall shear stress (WSS) distributions in both the phases decreased with increases in the dilation ratio, confirming the stenotic nature of low WSS^[21,22] (Figure S9, bottom, Supporting Information). Together, the time-averaged oscillatory shear index (OSI) decreased by ≈ 5 times w/ SES (≈ 0.01) compared with the index w/o SES (≈ 0.05) (Figure 3d); thus, the target dilation ratio to be maintained by SES was determined to 2.5.

2.4. Rabbit Model of AVF

The pore size and dilation ratio of microarchitecture of SES were set separately to promote beneficial inflammation and thereby minimize stenotic flow disturbance. Hence, the combined effects were validated by grafting a femoral vein segment in between a carotid artery as a form of artery–vein–artery (AVA) in rabbits w/ or w/o support deployment for 28 days (Figure 4a). As a specific control, a stiff poly(L-lactic acid) (PLLA) support (modulus: 1780 MPa) with the same baseline micropore architecture and design as those of SES (modulus: 2.66 MPa) was used to eliminate the effect of dilation-responsive microscale shape programming (Figure 4a). Indeed, compared to the w/o SES and PLLA groups, the SES deployment significantly reduced neointima formation by almost 75% and thereby decreased the intima to media ratio by approximately three times through markedly attenuation of vein dilation along with the efficient regeneration of vasa vasorum in the quantitative analysis of pentachrome images (Figure 4b; Figure S10, Supporting Information). The w/o SES group showed a marked difference between the in vivo result (>8 times; Figure 4b) and CFD values (3.5 times; Figure 3c). In this case, the CFD value of the w/o SES group was produced based on the input information from previous reports^[17–22] with the consideration of the results of ex vivo experiment (Figure 3b). In addition, the CFD analysis was performed a moment right after dilation without considering the fact that stenotic vessels undergo outward vein remodeling to dilate,^[23] thereby preserving the lumen area during the 4 weeks of implantation in the rabbit model. The degree (2.5 times) of w/ SES was calculated in the CFD analysis and maintained in the rabbit model more efficiently (2.5–3 times) compared to the w/o SES group. Considering the lumen closure of the PLLA deployment, these results indicate a key role of dilation-responsive microscale shape programming of SES in leading the antistenotic effect in vivo.

As further validation points in the rabbit model, i) SES clearly directed laminar flow formation in contrast to the oscillatory flow patterns w/o SES and closed lumen-mediated flow stoppage of PLLA groups, as shown by Doppler imaging

from day 0 to day 28 (Figure 4c). ii) The w/ SES group significantly induced CD206 expression (M2 marker), as opposed to the expression of inducible nitric oxide synthase (iNOS, M1 marker) at the protein levels, compared to the w/o SES group (Figure S11, Supporting Information). iii) The w/ SES group exhibited the intensified fluorescence signal of the SMC layer with more points of adventitial microvessels, compared to the w/o SES (Figure 4d), indicating muscle reinforcement like an artery instead of triggering venous intimal hyperplasia with effective regeneration of vasa vasorum. Notably, these parameters were not measurable in the PLLA groups owing to the structural collapse of the vessel layer.

2.5. Beagle Dog Model of AVF

As a preclinical model, beagle dogs were subjected to AVF so that the SES effect was confirmed by wrapping to cover the anastomosis part for 28 days (Figure 5a). SES wrapping reduced vein dilation continuously by more than 30% for 28 days, compared to the SES group (Figure 5b). As a result, the quantitative analyses of pentachrome and immunostaining images demonstrated that SES deployment significantly reduced neointima formation (area and intima to media ratio), with significant reinforcement of the vascular smooth muscle cell (VSMC) layer and vasa vasorum compared to the w/o SES group (Figure 5c,d; Figure S12, Supporting Information). These results agreed well with those in the in vitro and rabbit AVA grafting models. Strikingly, the Doppler images indicated that SES deployment promoted arterial flow formation (i.e., peak clarity and height of forth flow under red arrows), but reduced disturbed flow as presented by marked decreases in back flow, compared to the w/o SES group (Figure 5e).

3. Discussion

For the past 30 years, tremendous efforts have been applied to treat occlusive vascular remodeling in clinical and preclinical models of vascular grafting, stenting, hemodialysis access, etc. One particular trend in common for the approaches is to target a pathological event inside vessels. However, since all target events occur as parts of the pathological cascade and occur in a domino fashion,^[24,25] reversing the events back to a normal status by a therapeutic or surgical treatment in the middle of the process appears to be almost impossible. Moreover, there are inherent risks in any intravascular surgical treatment because the intravascular deployment of a device often induces formation of disturbed blood flow, and thereby triggers pathological vascular remodeling.^[26] Consequently, a series of downstream cascading events proceeds from endothelial dysfunction to foam cell formation, in collaboration with inflammatory signaling and lipid oxidation, further leading to aggressive SMC migration/proliferation, in turn leading to occlusive lesion formation.^[27,28] However, lipid-lowering drugs are still considered as a therapeutic winner,^[29,30] and the degree of vascular occlusion progressively increases over the years after a surgical treatment. Moreover, none of the reported out-wall attempts^[31,32] was successful in moving to an advanced translation stage

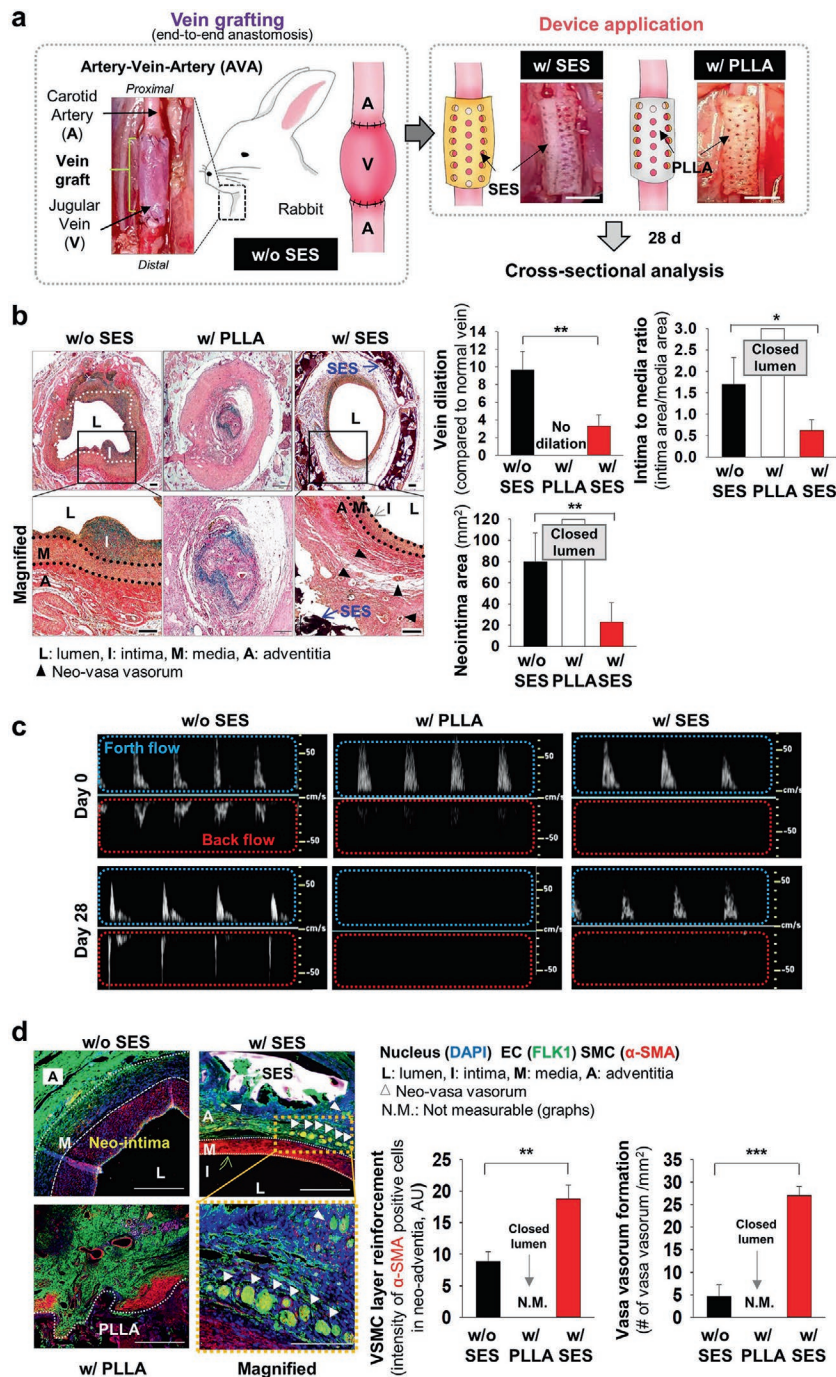


Figure 4. Application of the self-enclosable external support (SES) in a rabbit model of artery–vein–artery (AVA) grafting. a) Illustration of support (SES or PLLA) deployment procedure by wrapping a rabbit AVA graft in end-to-end anastomosis. SES was positioned at the vein graft site, covering both proximal and distal anastomosis points. Then, it self-enclosed to wrap the AVA graft by pouring warm water to increase the temperature near 40 °C (shape recovery point = T_m). Scale bar = 1 cm. b) (Left) Pentachrome staining images of cross-sectioned vein grafts w/ or w/o support (SES vs PLLA) deployment at day 28 postsurgery, followed by (right) quantitative image analysis of vein dilation, intima to media ratio, and neointima area (L: lumen, I: intima, M: media, and A: adventitia) ($N = 4$). c) Sonography confirmation of unidirectional (forth) flow w/ SES versus oscillatory (back and forth) flow w/ PLLA and w/o SES throughout vein grafts at day 0 and day 28 post-AVA surgery. Blue and red boxes indicate back and forth flow, respectively. d) (Left) Protein expression of Flk-1 (endothelial cell marker, green) and alpha smooth muscle actin (α -SMA, SMC marker, red) with nucleus (blue) in vein grafts w/

owing to the side-effects of partner drugs and insufficient elastic property (i.e., stiff or soft) to handle body movements (e.g., vessel dilation). Considering the aforementioned points, this study suggests an unprecedented solution by approaching the out-wall side of the vessel using a well-justified microscale shape programming of the external wrapping device (SES).

The micropore function was enabled by the cooperation of wrap (tube) shape recovery with the elastic property of SES material. Acquisition of the elastomeric property above T_m is part of shape memory properties and thus can be considered as a design factor for shape programming. As shown in the Movie S1 in the Supporting Information, the initial shape transition from the unwrapped, plate shape to the wrapped, tube shape (“shape memory”) provided the foundation to operate the following shape programming in a microscale based on the preanalyses of vein dilation parameters upon grafting (Figure 3; Figures S8 and S9, Supporting Information). In response to vein dilation, the elastomeric behavior of SES material above T_m as part of shape memory properties enabled the ellipsoidal expansion of large micropores with the consequent increase of the pore interconnectivity. Also, the vein dilation led to crushing of small micropores, thereby acting as void bridges to merge neighboring large pores. This cooperative procedure was defined as dilation-responsive microshape programming.

In this study, the SES design enabled the following functions and thereby validated the strategies of our approach. First, as a biotechnological point of view, inherent elastomeric properties of polycaprolactone (PCL)-based SMP together with tuning of both crosslinking degree and porosity, generated a vascular level (average modulus: 1.54 MPa per artery and 2–3 MPa per vein)^[33,34] of the modulus of SES (2.66 MPa) with the maximum strain at break among the test groups (Table S1, Supporting Information). Consequently, as determined in the ex vivo and computational models (Figure 3), wrapping vein grafts and anastomosis points by SES

or w/o support (SES or PLLA device) deployment at day 28 postsurgery. (Right) The intensity of α -SMA positive cells (left graph) and the number of neo-vasa vasorum (right graph) per neoadventitia area were quantitatively analyzed postimmunostaining (L: lumen, I: intima, M: media, and A: adventitia) ($N = 3$). Scale bar = 200 μ m. N.M.: not measurable. * $p < 0.05$, ** $p < 0.01$, and *** $p < 0.001$ between comparison groups.

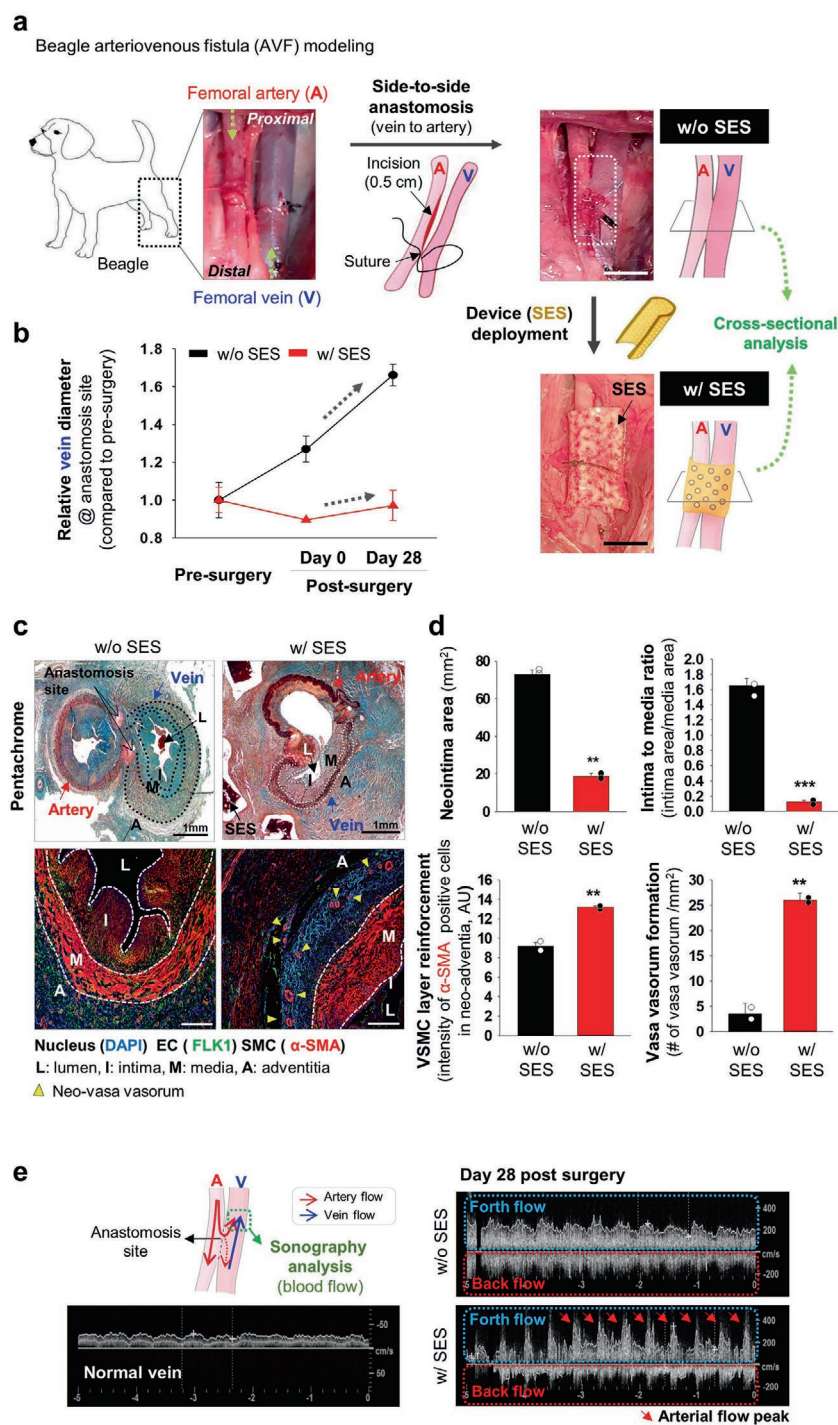


Figure 5. Beagle dog model of arteriovenous fistula (AVF) to confirm the antistenotic effects of SES. a) Illustration of the surgical processes to model AVF in beagle dogs ($N = 2$). First, the side-to-side anastomosis between femoral artery and vein was performed. Then, the SES was deployed to cover the vein and two anastomosis points by self-wrapping. Beagles were sacrificed at day 28 postsurgery for analysis. Scale bar = 1 cm. b) The vein diameter of AVF anastomosis site was measured before surgery as well as at day 0 and day 28 postsurgery. The values were normalized to that of presurgery (=1), thereby excluding the influence of initial diameter difference between the two groups on the comparison analysis. c) Histological images from pentachrome staining (top row: elastic fibers and nuclei, black; collagen, yellow; mucin, light blue; muscle, red) and immunofluorescence staining (bottom row: Flk-1 endothelial cell marker, green; alpha smooth muscle actin (alpha-SMA) SMC marker, red; DAPI nuclei

in the rabbit model of vein to artery grafting (end-to-end) controlled the volumetric expansion enough to synchronize graft motion with arterial contraction, thereby minimizing disturbed flow formation (Figure 3c). This function prevented neointima formation and the subsequent pathological cascade (Figure 4), which was confirmed in the canine model of artery-vein grafting (side-to-side) (Figure 5). A breakthrough point to emphasize here is that the computational modeling enabled prediction of the volumetric expansion degree of the vein to minimize disturbed flow formation, thereby proving the concept of approach (Figure 3).

Second, from a biological point of view, out-wall wrapping with a synthetic, biodegradable material induced acute inflammation and thereby guided SMC migration toward adventitia instead of the intima side (Figure 2). This inflammation appeared to be regenerative rather than destructive, as evidenced by M2 activation of macrophages, which also promoted vasa vasorum regeneration. During washing and preparation of vein to graft postharvest, vasa vasorum is damaged, resulting in hypoxic disorders and subsequent pathological phenotype switch of SMCs. The collaborative effects among regenerative inflammation, vasa vasorum regeneration, and porosity can rescue the ischemic disorders and induce migration of healthy SMCs toward adventitia. As a result, the vein graft was endowed with arterial properties in cooperation with the elastomeric support from SES.

Last, from a user point of view, surgeon-friendly deployment processes were enabled in alignment with the concept of precision medicine by temperature-responsive, automatic wrapping to the precalculated, vessel geometry-specific size and structure. SES undergoes shape transition upon shift in temperature to T_m , in which heat energy is transferred to activate the mobile phase for shape recovery. The shape recovery rate is a

counterstaining, blue) for the cross-sections of anastomosis sites w/ or w/o SES at day 28 postsurgery (L: lumen, I: intima, M: media, and A: adventitia). d) Quantitative analysis of images to determine neointima area, intima to media ratio, VSMC layer reinforcement, and vasa vasorum formation. Each dot represents each N of animal. Scale bar = 200 μ m. ** $p < 0.01$ and *** $p < 0.001$ versus w/o SES. e) Sonography analysis for vascular accessibility and blood flow pattern of the test groups (red arrow: arterial flow). The SES deployment markedly promoted arterial flow formation compared to the clear disturbed flow pattern (back and forth) of w/o SES group.

few seconds (Movie S1, Supporting Information) and tunable by controlling the thickness and crosslinking degree of the SES material.^[8] There was no evidence of instability of SES functions because of the ability to manage repeated stress ($\approx 20\,000$ times) in response to 10% cyclic strain at 37 °C (Figure 1c). Moreover, the Doppler and histology results from the rabbit (Figure 4) and canine (Figure 5) experiments indicated the functional and structural maintenance of SES at the body temperature (37 °C) during implantation period. Since this is the first trial to apply shape memory functions in this type of medical device, further works are needed, in collaboration with surgeons and clinicians, to maximize the benefits of self-wrapping (e.g., significant reduction of surgery time and risk of infection). Together, the three points of the design concept were validated in a canine model of side-to-side artery–vein grafting (Figure 5).

In this study, a simple intention toward a user-friendly means initiated the application of shape memory effect to enable self-wrapping of SES upon temperature shifting by treatment with warm water. The treatment temperature is tunable by reducing the crystallinity of PCL via the control of the crosslinking degree, as elaborated previously.^[8] The overall results indicate that the benefit of the shape memory properties is more impactful than the simple intention. The programming of wrapping shape can be used to operate the dilation-responsive actions of large and small micropores based on preanalyses of grafting type, pathological condition, geometry, diameter, and dilation degree depending on the surgical situation of vascular anastomosis. More importantly, the elastic shape fixity enabled repeated reset of programmed structural parameters in response to cyclic movement of vessels by regulating the dilation degree; thus, the unexplored aspect of vascular devices was approached to address the significant issues in side-to-side and end-to-end grafting of vessels, representing a meaningful advancement in the field.

Nonetheless, further studies are always inevitable in moving toward the final stage of translation. Our results establish that the elastic fixity of SES enables the handling of vein dilation to an appropriate degree, not only for doctors to find out a point of needle insertion during hemodialysis access but also for the dilated vein to minimize disturbance of blood flow. The elastic property of SES to manage repeated stress up to $\approx 20\,000$ times (Figure 1c) indicates a promising property of SES to synchronize with vessel contraction. As further evidenced by the superior results of SES in comparison with those of the stiff PLLA control, this robust management of elastic properties, in response to the artery contraction (10%)-mimetic cyclic strain, is required to minimize disturbance of vessel contraction and blood flow upon SES loading to pulsing vessels (Figures 4c and 5e). The results indicate that loading of a stiff material (e.g., PLLA) can exacerbate vessel stenosis by disturbing vessel contraction and flow pulsation (Figures 4c and 5e). However, in future studies, more in vitro and in vivo experiments are required to settle whether the property is continuously flexible enough to synchronize the device movement with dynamic contraction of the AVA graft under real blood flow.

Next, the reproducibility of porosity might not be guaranteed because of the nature of the porogen leaching process, although the number and location of punching could be controlled

during manufacturing. Hence, a 3D-printed mold is currently attempted to develop a mesh structure, thereby improving the reproducibility of the micropore structure and porosity. The model is designed using computer simulation and numerical analysis to distribute contraction-mediated stress uniformly on the mesh structure of SES. Therefore, the manufacturing process will be tuned to successfully undergo the approval process for clinical translation. As another aspect to investigate further, warm water was injected to activate the shape recovery of SES because saline irrigation of surgical site has been routinely performed in operation rooms, and thus, additional requirement of heating equipment can be minimized. In addition, electrical air heating may not transfer the heat energy to the entire device homogeneously and the body temperature decreases around a deployment site because of open surgery. Saline irrigation did not cause any significant issues (e.g., inflammation), as seen in the in vivo results (Figures 4 and 5). If soft tissues are burned, water temperature can be reduced by increasing the crosslinking degree with reduction of PCL crystallinity as shown in our previous study.^[8] However, the method will be optimized by discussing with users through clinical trials in the future.

4. Conclusion

This study represents a paradigm shift in approaching to prevent stenosis in vein-to-artery grafting using a SES. The effectiveness and advantages were demonstrated in a series of the results from material characterization, computational fluid dynamics, cell, rabbit, and dog experiments. SES was tuned to support arterial contraction and program the self-enclosable property. Wrapping anastomosis parts by SES adjusted mismatching of volumetric expansion and mechanical properties between vein and artery, thereby minimizing hemodynamic changes. Induction of beneficial inflammatory responses with the porous structure regenerated vasa vasorum postwashing damages and guided migration of smooth muscle cells toward the vascular wall, thereby rescuing ischemic disorders and promoting arterial properties, respectively. The results were promising enough to suggest this approach as a new solution for treatment of occlusive vascular remodeling in vein–artery grafting. Since the back and forth flow was not completely minimized in the current design, the y-shape grafting geometry and further tuning of material properties will be applied to the next design so that the disturbed flow formation can be minimized further, and consequently, the therapeutic effect can be promoted enough to move from bench to clinic. Indeed, SES serves as a foundation model to apply for risky situations such as coronary bypass grafting in the near future.

5. Experimental Section

Device Fabrication: The SMP, 94%polycaprolactone-co-06%polyglycidyl methacrylate (94%PCL-06%PGMA), was synthesized using the sequential process as described previously.^[35] To fabricate SES, 94%PCL-06%PGMA was dissolved in dichloromethane (DCM; D2863, Samchun Chemical Co., Seoul, Korea) at a concentration of 100 w/v% containing 0.1 w/v% of photoinitiator (Irgacure 2959, Ciba Specialty Chemicals Inc., Basel, Switzerland). Gelatin powder (MW 50–100 kDa; Sigma-Aldrich, St.

Louis, MO, USA) was used as a porogen to generate small micropores ($\approx 150 \mu\text{m}$ diameter). The SMP solution/gelatin mixture (1:1 volume ratio) was poured to fill the gap between the outer and inner mold tubes. For the rabbit model of vein-to-artery (end-to-end) grafting, SES was produced using Teflon tube (outer mold; O.D. = $\approx 5 \text{ mm}$ and I.D. = $\approx 4 \text{ mm}$) and silicone tube (inner mold; O.D. = $\approx 4 \text{ mm}$). Meanwhile, Teflon tube (outer mold; O.D. = $\approx 7 \text{ mm}$ and I.D. = $\approx 6 \text{ mm}$) and glass tube (inner mold; O.D. = 6 mm) were used to produce a device for the beagle model of AVF (side-to-side grafting model). Then, polymer crosslinking (recovery shape programming) was processed by exposing the samples to ultraviolet (UV) irradiation ($250\text{--}500 \text{ nm}$, 265 mW cm^{-2}) for 600 s in Omniscure S2000 (Lumen Dynamics Group Inc., Mississauga, Ontario, Canada), followed by $400 \mu\text{m}$ diameter punching (P) (3 pores mm^{-2}) to generate large micropores and washing for 5 days. To fabricate a control PLLA device for the rabbit model, PLLA (RESOMER L207S, Evonic Industries, Essen, Germany) was dissolved in DCM at a concentration of 15 w/v\% with addition of gelatin powder. The PLLA/gelatin mixture (1:1 volume ratio) was poured to the mold tubes with punching (3 pores mm^{-2}) to match the device size and pore architecture with those of SES before dilation.

Device Characterization: The thermal properties of SMP were characterized using differential scanning calorimeter (DSC; Discovery DSC25, TA instrument Inc., New Castle, DE, USA). The samples underwent two cycles of heating up to $150 \text{ }^\circ\text{C}$ and then cooling down until $-80 \text{ }^\circ\text{C}$ at $10 \text{ }^\circ\text{C min}^{-1}$ (heating/cooling rate). The crosslinking degree (%) was determined by measuring the dry weight of each sample before (m_{initial}) and after (m_{final}) dissolving in DCM for 2 h using the following Equation (1)

$$\text{Degree of crosslinking} = \frac{m_{\text{final}}}{m_{\text{initial}}} \times 100\% \quad (1)$$

The tensile modulus of each SMP film (5.5 mm (W) \times 40 mm (H) \times 0.6 mm (T)) with varying the porosity (1:0.5, 1:0.75, 1:1, and 1:1+P) or same size PLLA sample (1:1+P) was determined by a strain-controlled mode at a strain rate of $2\% \text{ min}^{-1}$ using dynamic mechanical analyzer (Discovery DMA850, TA instruments Inc., New Castle, DE, USA). In order to characterize fatigue properties, modulus of each SMP or PDMS film (5.5 mm (W) \times 40 mm (H) \times 0.6 mm (T)) without pores was measured with 10% strain-controlled fatigue with 3.4 Hz for $20\,000$ times at $37 \text{ }^\circ\text{C}$. Shape recovery ratio was determined by % of recovery from temporary deformation under $>10\%$ strain to original shape. A porous structure of SES sample was analyzed using the field emission scanning electron microscope (FE-SEM; MERLIN, Zeiss, Oberkochen, Baden-Württemberg, Germany). SES samples were vertically sectioned, coated with platinum (Pt), and then, subjected to FE-SEM imaging, followed by the quantitative analysis of pore percentage per total image area using Image J (ver. 1.52a, NIH, Bethesda, MD, USA).

Micropore Changes: Dilation-responsive structural changes (i.e., major and minor axial lengths and area) of large and small micropores were determined in a pressure-controllable flow model using a silicone tube and a syringe pump. One end of the silicone tube (O.D. = 2 mm) was tied, while the other end was connected to the syringe pump (88-3015, Harvard Apparatus, Holliston, MA, USA) by Luers (O.D. = 1.6 mm ; 45518-00/45508-00, Cole-Parmer, Vernon Hills, IL, USA). Then, each SES sample with the temporary shape (Tem) was placed on the silicone tube and set to wrap the tube (shape recovery), followed by water injection by the syringe to the tube until 2.5 times dilation was reached (dilated shape: Dil).

SES samples of Tem and Dil stages were stained with $100 \mu\text{g mL}^{-1}$ fluorescein (46955, Sigma-Aldrich, St. Louis, Missouri, USA) for 3 min and subjected to confocal laser scanning (LSM780, Zeiss, Oberkochen, Land Baden-Württemberg, Germany), followed by quantitative image analysis using Image J software (ver. 1.52a). The analyzed parameters were thickness of SES sample as well as major/minor axial length and area of large and small micropores.

Micropore Interconnectivity: The average diameters (Tem = $400 \mu\text{m}$ and Dil = $500 \mu\text{m}$) of SES micropores were determined by confocal imaging, and a membrane form of porous Tem or Dil SES was produced by punching the corresponding pore size. Each membrane sample was placed onto the strainer filter, and the following experiment was

carried out at room temperature to exclude any effect of temperature shift on transport of fluorescein isothiocyanate-conjugated dextran (FITC-dextran). FITC-dextran (1 mg mL^{-1} , MW 40 000, 4.5 nm , FD40S) particles were loaded onto the strainer column and centrifuged down through micropores of the test membrane (z-directional transportation) for 30 s using QIAamp Mini Spin Columns (1000 rpm , 51304, Qiagen, Hilden, Germany). The transported FITC-dextran particles were collected, and the corresponding fluorescence intensity as an indication of pore interconnectivity was measured using a fluorescence plate reader (SpectraMax 340, MolecularDevice Co., San Jose, CA, USA).

FACS: Raw 264.7 macrophages (ATCC, Manassas, VA, USA) were attached on test substrates (coverslip, flat SMP, and porous SMP) overnight and activated by treatment of LPS (100 ng mL^{-1} ; L4391, Sigma-Aldrich, St. Louis, Missouri, USA) for 3 days. The samples were fixed with 4% paraformaldehyde (PFA; 3025-89-4, Sigma-Aldrich, St. Louis, Missouri, USA) for 15 min, permeabilized using 0.3% Triton X-100 (93443, Sigma-Aldrich, St. Louis, Missouri, USA) for 15 min, and blocked using 5% bovine serum albumin (BSA; 82-100-6, Millipore, Burlington, MA, USA) for 1 h. Samples were then incubated with primary antibodies ($1:100$ dilution, CD68; ab31630, iNOS; ab15323, and CD206; ab64693, Abcam, Cambridge, Cambridgeshire, UK) in 5% BSA for 1 h, washed three times with PBS (LB004-02, Welgenc, Gyeongsan, Korea), and treated with secondary antibodies ($1:200$ dilution, Alexa Fluor 488; 115-545-144 and Alexa Fluor 594; 111-585-003, Jackson ImmunoResearch Laboratories, West Grove, PA, USA) in 5% BSA for 1 h in the dark, followed by washing three times with PBS. Finally, cells were suspended in PBS and subjected to the FACS analysis (LSR Fortessa, BD, Franklin Lakes, NJ, USA) and analyzed using FlowJo (FlowJo V10, BD, Franklin Lakes, NJ, USA).

Gene Expression: Quantitative real-time polymerase chain reaction (qRT-PCR) was used to determine gene expression of i) interleukin (IL)-10 and IL-4 for regenerative inflammation, ii) IL-1 β and monocyte chemoattractant protein (MCP)-1 for proangiogenesis, and iii) platelet-derived growth factor (PDGF)- β and insulin-like growth factor (IGF)-1 for VSMC migration. Total RNA of each group was extracted using 1 mL TRIzol reagent (7817, Invitrogen, Waltham, MA, USA). RNA ($1 \mu\text{g}$) was dissolved in diethyl pyrocarbonate (DEPC) water to synthesize complementary DNA (cDNA) using AccuPower CycleScript RT Premix (K-2044-B, Bioneer, Daejeon, Korea). StepOne Plus Real-Time PCR (Applied Biosystems, Waltham, MA, USA) was conducted with cDNA using SYBR Green PCR master mix (4367659, Thermo Fisher Scientific, Waltham, MA, USA). The expression level of each gene type was normalized to that of glyceraldehyde 3-phosphate dehydrogenase (GAPDH) as a housekeeping gene and analyzed using the relative quantification $2^{-\Delta\Delta\text{CT}}$ method.

SMC Migration: The effect of SES to trigger vascular SMC migration was determined using a Radius cell migration assay (CBA-125, Cell Biolabs, San Diego, CA, USA) and a Boyden Chamber assay (CBA-106, Cell Biolabs, San Diego, CA, USA) following the instructions of the manufacturer. CM were obtained from the 3-day culture of Raw 264.7 (5×10^5 cells per well) on the test substrates (coverslip, flat SMP, and porous SMP) under the LPS treatment (100 ng mL^{-1}). For the Radius cell migration assay, human aortic SMCs (2×10^5 cells per well) were seeded into a specialized 24-well plate (112501, Cell Biolabs, San Diego, CA, USA) in which a biocompatible hydrogel (Radius gel, diameter = $0.68 \text{ mm} \pm 0.014 \text{ mm}$; 112502, Cell Biolabs, San Diego, CA, USA) was positioned in the center of each well. After culturing for a day, this gel was removed using Radius Gel Removal Solution (112504, Cell Biolabs, San Diego, CA, USA) so that the cell-free region was exposed in the center spot where the gel was removed. The three types of test CMs were treated to SMCs, and their migration was observed at 0, 4, 12, and 24 h using the fluorescence microscope (DMI 8, Leica, Wetzlar, Hesse, Germany) postnucleus staining with 4',6-diamidino-2-phenylindole (DAPI) (112002, Cell Biolabs, San Diego, CA, USA). The number of cells in the cell-free center region was counted using the Image J software (ver. 1.52a). The Boyden Chamber assay was conducted in a 96-well plate, in which a membrane chamber (upper side, $8 \mu\text{m}$ pore size) and a feeder tray (bottom side) were equipped. CM were

filled in the feeder tray; the membrane chamber was placed onto the tray; and then, SMCs (2×10^4 cells per well) were seeded and cultured on the membrane chamber with endothelial cell growth medium-2 (EGM-2; CC-3162, Lonza, Basel, Switzerland) without serum for 24 h. SMCs migrated through the membrane pore and reached underneath the membrane chamber. SMCs (no migration) at the seeding face of the membrane were removed, and only SMCs (migration) underneath the membrane were dissociated from the membrane using the cell detachment buffer (10403, Cell Biolabs, San Diego, CA, USA), followed by cell lysis using lysis buffer (10404, Cell Biolabs, San Diego, CA, USA). The cell number was quantified by staining with CyQuant GR fluorescent dye (10105, Cell Biolabs, San Diego, CA, USA) and then measuring the fluorescence intensity at 480 nm/520 nm in a fluorescence plate reader (SpectraMax 340, MolecularDevice Co., San Jose, CA, USA).

EC Tube Formation: CM were obtained from a 3-day culture of Raw 264.7 on the test substrates (coverslip, flat SMP, and porous SMP) under the LPS treatment (100 ng mL^{-1}). Next, human umbilical vein endothelial cells (HUVECs, 2×10^5 cells per well) were seeded on Matrigel (354230, Corning Inc., Corning, NY, USA) in 24-well plates and cultured under the CM treatment at 37°C and $5\% \text{ CO}_2$ for a day. HUVECs were stained with Alexa 488 labeled-phalloidin (A12379, Invitrogen, Waltham, MA, USA) and imaged using the confocal laser scanning microscope (LSM780, Zeiss, Oberkochen, Land Baden-Württemberg, Germany), followed by the image analysis using Image J (ver. 1.52a).

Ex Vivo Vein Dilation: Reduction of vein dilation based on the SES deployment was examined in an ex vivo model where vein dilation with (w/) versus without (w/o) SES was profiled in response to increases in the water injection pressure caused by a syringe (Figure 4b). One end of the rabbit jugular vein (2 cm) w/ or w/o SES was tied using the 10-0 nylon suture (W2814, Ethicon, Somerville, MA, USA), while the other end was tied in connection with a syringe pump (88-3015, Harvard Apparatus, Holliston, MA, USA) using male/female Luers (O.D. = 1.6 mm; 45518-00/45508-00, Cole-Parmer, Vernon Hills, IL, USA) and silicone tube (I.D. = 1 mm, O.D. = 2 mm; SL-0102, LK LAB Korea, Namyangju, Korea). A pressure gauge (hydraulic meter; TST-10.0, TIVAL Sensors GmbH Co., Wuppertal, Rhine-Westphalia, Germany) was positioned between the syringe pump and test samples, and then, water was injected (1 mL min^{-1}) into test veins using the syringe (5 mL volume). Changes in the vein diameters were profiled in response to increases in the water injection pressure (mmHg).

Computational Modeling: Hemodynamic parameters of the vein region in the rabbit model of AVA grafting were predicted using CFD. First, the model was assumed to be a simple straight structure with an artery with a diameter of 1 mm and a vein with a length of ≈ 10 mm. The dilation ratio was varied to 1.0, 1.5, 2.0, 2.5, 3.5, and 5.0, and CFD was conducted using the CFX module with the ANSYS software (ANSYS 2019; ANSYS, Canonsburg, PA, USA). The mesh dependency of the calculated results was tested in advance so that a sufficient number of hexahedron meshes was generated for each model, resulting in 580 000–670 000 mesh elements. The characteristic parameters of normal blood (i.e., $40.08 \text{ kg mol}^{-1}$ molar mass and 1060 kg m^{-3} density) were incorporated into the CFD analysis. Non-Newtonian viscosity was expressed using the Carreau–Yasuda model with the low shear viscosity (0.022 Pa s), high shear viscosity (0.0022 Pa s), time constant (0.11 s), power law index (0.392), and Yasuda exponent (0.64421).^[36] A completely nonslip wall boundary condition was applied over the entire AVA wall domain, and an open boundary condition was assumed in the outlet. Subsequently, the SST $k-\omega$ turbulence model was applied to tailor the nonlaminar behavior of blood flow despite the nature of flow in the models is likely to be laminar owing to the slow flow velocity and small vessel diameter.

Rabbit VG Model: All animal experiments and management procedures were approved by the Institutional Animal Care and Use Committee (IACUC) of the Yonsei Laboratory Animal Research Center (YLARC) (Permit No. 2017-0351). New Zealand rabbits (male 7–8 months old; Orient Inc., Seongnam, Korea) with a weight of 3.0 kg were anesthetized with Alfaxan (5 mg kg^{-1} ; Jurox, Hunter Valley, New South Wales, Australia) and Xylazine (5 mg kg^{-1} ; Bayer Korea, Seoul, Korea) by an intramuscular injection and maintained by the endotracheal intubation

of 2% isoflurane during surgery. The AVA (vein interposition) modeling was processed by grafting a jugular vein segment into a precut part of the carotid artery with end-to-end anastomosis. Briefly, i) proximal and distal sites of external jugular vein and carotid artery were temporarily clamped with clamps; ii) a jugular vein segment (≈ 1 cm) was obtained by dissecting both the ends of the jugular vein between the clamps; and iii) the vein segment was grafted in between the precut ends of the artery using end-to-end anastomosis that includes simple interrupted 10-0 nylon suturing (W2814, Ethicon, Somerville, MA, USA). After the anastomosis, the entire vein grafts were wrapped w/SES or left w/o SES as sham control. And then, the clamps were removed to perfuse blood flow. At day 28 postsurgery, the vein grafts were harvested for further analysis.

Canine AVF Model: All animal experiments and management procedures were approved by the IACUC of the Wonju College of Medicine, Yonsei University (Permit No. YWC-190524-1). Beagle dogs (male 8–10 kg, Dae Han Bio Link Co., Eumseong-gun, Korea) were anesthetized by the intramuscular injection of ketamine (5 mg kg^{-1} ; Ketamine 50, Yuhan, Seoul, Korea) and maintained by endotracheal intubation of Isotroy (Troikaa Pharmaceuticals Ltd., Ahmedabad, Gujarat, India) during surgery. AVF was modeled in both the back hind thighs (left: w/ SES; right: w/o SES) in each beagle ($N = 2$). First, an incision (5 cm) was made into the center of the skin in each thigh, underlying subcutaneous tissues were then removed, and the femoral artery and vein were exposed. Second, the proximal and distal parts of the femoral artery and vein were clamped (RS 5459, Roboz Surgical Instrument Co., Gaithersburg, MD, USA), thereby securing a surgical site (2–3 cm) in each back thigh. Third, an incision (≈ 0.5 cm) was made into the side wall of each artery and vein vessel, followed by side-to-side anastomosis through suturing with silk 6-0 (G-1, Ethicon, Somerville, MA, USA). Finally, the two anastomosed sites (proximal and distal) and the entire vein graft were wrapped w/ SES in the left thigh, whereas the parts of the right thigh were left w/o SES as a sham control. The skin of surgical site was sutured with prolene 4-0 (W211, Ethicon, Somerville, MA, USA). Since then, the dilated diameter of vein graft in each thigh was measured every week using sonography (NextGen LOGIQ, GE Medical Systems Co., Chicago, IL, USA). At day 28 postsurgery, beagles were sacrificed using potassium chloride (KCl; 20 mg kg^{-1} ; Choongwae Pharma Corporation, Seoul, Korea) under general anesthesia using ketamine (5 mg kg^{-1} ; Ketamine 50, Yuhan, Seoul, Korea), followed by harvesting an arteriovenous tissue (3 cm) on the surgical site of each group for further analysis.

Histological Analysis: Harvested vein grafts were washed using saline and fixed for a day in 10% neutral buffered formalin (F2013, Biosesang, Seongnam, Korea). The samples were then embedded in paraffin wax and cross-sectioned to $5 \mu\text{m}$ thick slices. The pathohistological analysis of slices was performed with Movat's pentachrome staining (Russell-Movat Pentachrome stain kit, KTRMP, American MasterTech, Lodi, CA, USA). Deparaffinized slices underwent a series of reactions with i) Verhoeff's stain solution for 10 min, ii) 1% Alcian blue stain solution for 20 min, iii) crocein scarlet-acid fuchsin for 2 min, iv) alcoholic saffron solution for 15 min, and were v) finally imaged by microscope. Hematoxylin and eosin (H&E) staining was conducted on deparaffinized slices (hematoxylin for 3 min and eosin for 30 s). The images were quantitatively analyzed using Image J (ver. 1.52a) to determine the diameter of the vein, neointima formation (neointima area and intima to media ratio), and vasa vasorum formation in each test group.

Immunofluorescence Staining: Sample slides were reused by retrieving antigen through heating with citrate buffer treatment (C9999, Sigma-Aldrich, St. Louis, MO, USA). The slides were permeabilized with 0.3% Triton X-100 (93443, Sigma-Aldrich, St. Louis, MO, USA) in PBS for 15 min and blocked with 5% BSA for an hour. The sample slides were incubated with primary rabbit anti-Flk-1 (1:100 dilution; sc504, Santa Cruz Biotechnology, Dallas, TX, USA) and mouse anti- α -SMA (1:100 dilution; ab7817, Abcam, Cambridge, Cambridgeshire, UK) antibodies for 3 h. Then, the slides were washed with PBS containing 0.5% Tween 20 and reacted with secondary antirabbit conjugated to Alexa Fluor 488 (1:200 dilution; 115-545-144, Jackson ImmunoResearch Laboratories, West

Grove, PA, USA) and antimouse conjugated to Alexa Fluor 594 (1:200 dilution; 111-585-003, Jackson ImmunoResearch Laboratories, West Grove, PA, USA) for 1 h. Cell nuclei were counterstained with NucBlue Live ReadyProbes reagents (7817, Invitrogen, Waltham, MA, USA) for 5 min. The samples were imaged using the confocal laser scanning microscope (LSM780, Zeiss, Oberkochen, Land Baden-Württemberg, Germany) with quantitative analysis using Image J (ver. 1.52a).

Statistical Analysis: Statistical significances between w/ and w/o SES vein grafted groups were performed with unpaired Student's *t*-test statistical significances. One-way analysis of variance (ANOVA) with Tukey's significant difference posthoc test was used for the quantitative data of shape recovery temperature and porosity of SES, gene expression level in macrophages, in vitro EC tubulogenesis, and VSMC migration. All analyses were performed using SigmaPlot 12.0 (Systat Software Inc., San Jose, CA). The results were presented as mean ± standard deviation, and statistical significances of **p* < 0.05, ***p* < 0.01, and ****p* < 0.001 were considered.

Supporting Information

Supporting Information is available from the Wiley Online Library or from the author.

Acknowledgements

S.W.Y., Y.M.S., and J.B.L. contributed equally to this work. This study was financially supported by the National Research Foundation of Korea (NRF) (2016M3A9E9941743 and 2019R1A2C2010802), the Technology development Program (S2851324) funded by the Ministry of SMEs and Startups (MSS, Korea), and the Korean Medical Device Development Fund grant funded by the Korea government (the Ministry of Science and ICT, the Ministry of Trade, Industry and Energy, the Ministry of Health & Welfare, the Ministry of Food and Drug Safety) (Project Number: 2020M3E5D8104981).

Conflict of Interest

The authors declare no conflict of interest.

Data Availability Statement

The data that support the findings of this study are available from the corresponding author upon reasonable request.

Keywords

dilation-responsive, microscale shape programming, self-enclosable external support, shape-fixity, vein-to-artery grafting

Received: November 19, 2020

Revised: February 2, 2021

Published online: March 17, 2021

[1] M. Montgomery, S. Ahadian, L. Davenport Huyer, M. Lo Rito, R. A. Civitarese, R. D. Vanderlaan, J. Wu, L. A. Reis, A. Momen, S. Akbari, A. Pahnke, R. K. Li, C. A. Caldarone, M. Radisic, *Nat. Mater.* **2017**, *16*, 1038.

- [2] D. N. Ghista, F. Kabinejadian, *Biomed. Eng. Online* **2013**, *12*, 129.
 [3] S. V. Deo, *Ann. Thorac. Surg.* **2014**, *98*, 1142.
 [4] S. Bose, M. Roy, A. Bandyopadhyay, *Trends Biotechnol.* **2012**, *30*, 546.
 [5] C. Hudson, T. E. Kimura, A. Duggirala, G. B. Sala-Newby, A. C. Newby, M. Bond, *Sci. Rep.* **2018**, *8*, 4904.
 [6] R. Lorusso, G. Mariscalco, E. Vizzardi, I. Bonadei, A. Renzulli, S. Gelsomino, *Ann. Thorac. Surg.* **2014**, *97*, 2219.
 [7] M. R. Bennett, S. Sinha, G. K. Owens, *Circ. Res.* **2016**, *118*, 692.
 [8] Y. C. Shin, J. B. Lee, D. H. Kim, T. Kim, G. Alexander, Y. M. Shin, J. Y. Park, S. Baek, J. K. Yoon, Y. J. Lee, G. M. Seon, M. H. Lee, M. L. Kang, W. S. Jang, J. C. Park, H. W. Jun, Y. Kim, H. J. Sung, *Adv. Mater.* **2019**, *31*, 1904476.
 [9] K. J. Regehr, M. Domenech, J. T. Koepsel, K. C. Carver, S. J. Ellison-Zelski, W. L. Murphy, L. A. Schuler, E. T. Alarid, D. J. Beebe, *Lab Chip* **2009**, *9*, 2132.
 [10] L. R. Madden, D. J. Mortisen, E. M. Sussman, S. K. Dupras, J. A. Fugate, J. L. Cuy, K. D. Hauch, M. A. Laflamme, C. E. Murry, B. D. Ratner, *Proc. Natl. Acad. Sci. USA* **2010**, *107*, 15211.
 [11] V. Karageorgiou, D. Kaplan, *Biomaterials* **2005**, *26*, 5474.
 [12] M. Anghelina, P. Krishnan, L. Moldovan, N. I. Moldovan, *Stem Cells Dev.* **2004**, *13*, 665.
 [13] N. Jetten, S. Verbruggen, M. J. Gijbels, M. J. Post, M. P. De Winther, M. M. Donners, *Angiogenesis* **2014**, *17*, 109.
 [14] N. R. Patel, M. Bole, C. Chen, C. C. Hardin, A. T. Kho, J. Mih, L. Deng, J. Butler, D. Tschumperlin, J. J. Fredberg, R. Krishnan, H. Koziel, *PLoS One* **2012**, *7*, e41024.
 [15] J. Li, Y. Li, B. Gao, C. Qin, Y. He, F. Xu, H. Yang, M. Lin, *Nanomedicine* **2018**, *13*, 555.
 [16] M. L. Previtiera, A. Sengupta, *PLoS One* **2015**, *10*, e0145813.
 [17] M. R. de Leval, P. Kilner, M. Gewillig, C. Bull, *J. Thorac. Cardiovasc. Surg.* **1988**, *96*, 682.
 [18] D. L. Packer, P. Keelan, T. M. Munger, J. F. Breen, S. Asirvatham, L. A. Peterson, K. H. Monahan, M. F. Hauser, K. Chandrasekaran, L. J. Sinak, D. R. Holmes Jr., *Circulation* **2005**, *111*, 546.
 [19] J. J. Chiu, S. Chien, *Physiol. Rev.* **2011**, *91*, 327.
 [20] P. E. Vincent, A. M. Plata, A. A. Hunt, P. D. Weinberg, S. J. Sherwin, *J. R. Soc., Interface* **2011**, *8*, 1708.
 [21] K. S. Heo, K. Fujiwara, J. Abe, *Mol. Cells* **2014**, *37*, 435.
 [22] X. Li, B. Sun, H. Zhao, X. Ge, F. Liang, X. Li, J. Xu, X. Liu, *Sci. Rep.* **2018**, *8*, 5493.
 [23] M. R. Ward, G. Pasterkamp, A. C. Yeung, C. Borst, *Circulation* **2000**, *102*, 1186.
 [24] M. A. Gimbrone Jr., G. Garcia-Cardena, *Circ. Res.* **2016**, *118*, 620.
 [25] A. J. Lusis, *Nature* **2000**, *407*, 233.
 [26] K. Van der Heiden, F. J. Gijsen, A. Narracott, S. Hsiao, I. Halliday, J. Gunn, J. J. Wentzel, P. C. Evans, *Cardiovasc. Res.* **2013**, *99*, 269.
 [27] K. Yahagi, F. D. Kolodgie, F. Otsuka, A. V. Finn, H. R. Davis, M. Joner, R. Virmani, *Nat. Rev. Cardiol.* **2016**, *13*, 79.
 [28] M. R. de Vries, K. H. Simons, J. W. Jukema, J. Braun, P. H. Quax, *Nat. Rev. Cardiol.* **2016**, *13*, 451.
 [29] J. S. Kim, J. H. Kim, D. H. Shin, B. K. Kim, Y. G. Ko, D. Choi, Y. Jang, M. K. Hong, *Arterioscler., Thromb., Vasc. Biol.* **2015**, *35*, 2460.
 [30] K. Pahan, *Cell. Mol. Life Sci.* **2006**, *63*, 1165.
 [31] M. S. Conte, H. M. Nugent, P. Gaccione, I. Guleria, P. Roy-Chaudhury, J. H. Lawson, *J. Vasc. Surg.* **2009**, *50*, 1359.
 [32] V. Fuster, P. Charlton, A. Boyd, *Hum. Gene Ther.* **2001**, *12*, 2025.
 [33] F. Pukacki, T. Jankowski, M. Gabriel, G. Oszkinis, Z. Krasinski, S. Zapalski, *Eur. J. Vasc. Endovasc. Surg.* **2000**, *20*, 21.
 [34] J. C. Kohn, M. C. Lampi, C. A. Reinhart-King, *Front. Genet.* **2015**, *6*, 112.
 [35] J. Y. Park, J. B. Lee, W. B. Shin, M. L. Kang, Y. C. Shin, D. H. Son, S. W. Yi, J. K. Yoon, J. Y. Kim, J. S. Ko, C. S. Kim, J. S. Yoon, H. J. Sung, *Acta Biomater.* **2019**, *101*, 273.
 [36] J. Kwack, A. Masud, *Comput. Mech.* **2014**, *53*, 751.